Two-dimensional treesph simulations of choked flow systems

J. Klapp[a,1], L. Di G. Sigalotti[b,2], S. Galindo[a,3], and E. Sira[b,4]
[a]*Departamento de Física, Instituto Nacional de Investigaciones Nucleares, Km. 36.5 Carretera México-Toluca, 52045 Estado de México, México.*
[b]*Centro de Física, Instituto Venezolano de Investigaciones Científicas, Apartado Postal 21827, Caracas 1020A, Venezuela.*
e-mail: [1]*klapp@nuclear.inin.mx,* [2]*lsigalot@cassini.ivic.ve,*
[3]*sgu@nuclear.inin.mx,* [4]*esira@hubble.ivic.ve.*

Recibido el 1 de septiembre de 2004; aceptado el 19 de agosto de 2005

It is well-known that the flow of gas, liquid, and their mixtures through restrictors installed in pipeline systems is of great practical importance in many industrial processes. In spite of its significance, numerical hydrodynamics simulations of such flows are almost non-existent in the literature. Here we present exploratory two-dimensional calculations of the flow of a viscous, single-phase fluid through a wellhead choke of real dimensions, using the method of Smoothed Particle Hydrodynamics (SPH) coupled with a simple isothermal equation of state for description of the flow. The results indicate that an approximately stationary mean flow pattern is rapidly established across the entire tube, with the density and pressure dropping and the flow velocity rising within the choke throat. If the downstream flow is inhibited at the outlet end of the tube, a pressure drop of about 12% occurs across the choke when the mean flow reaches an approximate steady state. If, on the other hand, the flow is not inhibited downstream, the pressure drop is reduced to about 8% or less. The flow across the choke throat remains subsonic with typical velocities of $\sim 0.1c$, where c denotes the sound speed. In contrast, the flow velocities in the upstream and downstream sections of the pipe are on the average factors of ~ 6 and ~ 3.5 times lower, respectively. Correlation studies based on experimental data indicate that the pressure drop is only 3% or even less for gas flow through wellhead chokes at a speed of $0.1c$. This discrepancy reflects the inadequacy of the isothermal equation of state to describe realistic gas flows.

Keywords: SPH; numerical particle metnods; choked flow; compressible flow.

Es bien conocido que el flujo de gas, líquido y sus mezclas a través de restrictores instalados en sistemas de tuberías es de gran importancia práctica en muchos procesos industriales. A pesar de su importancia, simulaciones hidrodinámicas numéricas de este tipo de flujos son casi inexistentes en la literatura. Aquí presentamos cálculos exploratorios bidimensionales de flujo viscoso de una sola fase a través de un estrangulador de dimensiones reales, utilizando el Método de Hidrodinámica de Partículas Suavizadas (SPH) acoplado con una ecuación sencilla isotérmica de estado para la descripción del flujo. Los resultados indican que un patrón de flujo medio aproximadamente estacionario se establece rápidamente a través de todo el tubo, con la densidad y presión cayendo y el flujo de velocidad aumentando dentro del estrangulador. Si el flujo aguas abajo es inhibido a la salida del tubo, una caída de presión de alrededor de 12% ocurre a través del estrangulador cuando el flujo medio alcanza un estado aproximadamente estacionario. Si, por otro lado, el flujo no es inhibido aguas abajo, la caída de presión se reduce a 8% o menos. El flujo a través del estrangulador se mantiene subsónico con velocidades típicas de $\sim 0.1c$, donde c denota la velocidad del sonido. En contraste, la velocidad del flujo en las secciones aguas arriba y abajo del tubo son en promedio factores de ~ 6 y ~ 3.5 veces menores, respectivamente. Estudios de correlación basados en datos experimentales indican que la caída de presión es de solo 3% o inclusive menos para flujo de gas a través del estrangulador de la cabeza de un pozo a una velocidad de $0.1c$. Esta discrepancia refleja que la ecuación isotérmica de estado no es adecuada para describir flujos realistas de gas.

Descriptores: SPH; métodos numéricos de partículas; flujo estrangulado; flujo compresible.

PACS: 47.11.+j; 47.27.-i; 47.85.Dh

1. Introduction

The flow of gas-liquid mixtures through restrictors, such as flow control valves and chokes, in pipeline systems is of great practical interest in many applied branches of engineering. In the oil industry, wellhead chokes are installed to control flow rates and protect the surface equipment from unusual pressure fluctuations. Due to its practical significance, single-phase and two-phase flows through chokes have been the subject of numerous investigations in the past 40 years. However, the complexity of the problem has limited the investigation mostly to the development of empirical correlations based on experimental measurements and theoretical studies based on simplified treatments [1–6]. In general, when a flowing mixture crosses a choke, its velocity increases and its pressure drops. The empirical correlations aimed at predicting the dependence of the pressure drop on the velocity through the choke are usually valid over the range where experimental data are available, but may fail when extrapolated to new conditions. Also, existing correlations of oil, gas, and water show little success in describing the conditions that determine the boundary between critical and subcritical flow of multiphase mixtures through chokes. Therefore numerical hydrodynamics simulations aimed at predicting the flow properties through wellhead chokes for real conditions are highly desirable. With the exception of a very few instances [7], such simulations are practically non-existent in the literature, even for the case of single phase flows.

In this paper, we search for a way of solving the Navier-Stokes equations in order to simulate the flow of a single-

phase, viscous fluid through a wellhead choke using a modified version of the TREESPH method, originally introduced by Hernquist & Katz [8]. In particular, a Smoothed Particle Hydrodynamics (SPH) formulation is used which has been shown to produce accurate results for both compressible flows at high and moderate Reynolds numbers, and incompressible flows at low Reynolds numbers, without the need of special modifications [9]. Unlike other SPH-based schemes for treating viscous flows [10–13], the present method strictly relies on symmetrized SPH representations for the equations of motion and energy coupled with the usual kernel smoothing for the density. This results in a variationally consistent SPH scheme in which momentum preservation can be addressed properly [14]. The treatment of viscosity, thermal conduction, kernel interpolation, and boundary conditions are described in Refs. 9, 7 and 15 for a variety of different test cases including Poiseuille flow through parallel plates and Hagen-Poiseuille flow through a circular pipe, single phase flow through wellhead chokes, and formation of a stable liquid drop for a van der Waals fluid.

In this paper, with the aim of quantifying the pressure drop experienced by the flow across the choke throat, exploratory two-dimensional simulations of flow through a wellhead choke device of dimensions similar to those operating in real production tubing are presented. As a first approach, we neglect heat exchange between different parts of the fluid and assume an isothermal equation of state. Under this assumption, the flow is completely described by solving the continuity and momentum equations. Further work in this line will extend the present calculations to consider the flow of gas-liquid mixtures with more realistic equations of state. In particular, predictions of the pressure drop for two-phase flows through chokes are of fundamental importance because they will allow direct comparison with available correlation analyses of existing experimental data sets for both critical and subcritical flows of air/water, air/kerosene, natural gas, natural gas/oil, natural gas/water, and water flows (see Ref. 6), which predict on average a discharge coefficient of order unity when all data are considered simultaneously.

For the time-dependent plane Poiseuille test case described in Sec. 2.3 we have used a very low Reynolds number of $Re = 0.0125$, and for the choke models $Re \sim 10^6$. This high value for Re is due to the particular adopted isothermal equation of state. The choke dimensions used for the calculations are in accordance with typical real dimensions in oil pipeline systems. For more realistic equations of state for oil/gas mixtures, Re will be much lower. The SPH code used for obtaining the present results is based on an astrophysical code which has been tested for large Reynolds numbers for standard test cases and various astrophysical applications (see Sigalotti & Klapp [16] and cited references). Numerical SPH calculations of plane Poiseuille and Hagen-Poiseuille Flows for higher Reynolds numbers than ours have been performed by Takeda *et al.* [17], Morris *et al.* [13], Watkins *et al.* [12] and Sigalotti *et al.* [9].

2. Computational method

SPH is a fully Lagrangian technique for solving the partial differential equations of fluid mechanics in which the fluid elements are sampled and represented by particles. In its original form [18, 19], the method was developed for applications to astrophysical problems involving compressible flows [20–24]. Because of its wide range of applicability, SPH has also been employed to model industrial and natural processes, many of which often involve incompressible flows and their interaction with free and solid boundary surfaces [7, 9, 10, 15, 17, 25–27].

2.1. SPH equations and methodology

In SPH, the physical properties of a particle are determined from those of a finite number of neighboring particles through kernel interpolation. In this way, the value of any field quantity is represented by a weighted sum over the contributions of all neighboring particles. For instance, the continuous density field at the location of particle "a" is estimated according to

$$\rho_a = \sum_{b=1}^{N} m_b W_{ab}, \tag{1}$$

where m_b is the mass of particle b and the summation is taken over N neighboring particles, including particle a. The smoothing kernel or weight function $W_{ab} = W(|\mathbf{r}_a - \mathbf{r}_b|, h)$ depends on the distance between the particles and the smoothing length h specifying the extent of the averaging volume. The particles move with the local fluid velocity and, in addition to their mass, they carry other fluid properties specific to a given problem. With the smoothed representation of the fluid variables and their spatial derivatives, the continuum partial differential equations are converted into a set of ordinary differential equations for each particle.

In SPH formulations where Eq. (1) is used to replace the equation of continuity, variational consistency requires writing the SPH representations of the equations of motion and energy in symmetrized form [9, 14]. In particular, the symmetrized form used for the conservation of momentum is

$$\frac{d\mathbf{v}_a}{dt} = \sum_{b=1}^{N} m_b \left(\frac{S_a^{ij}}{\rho_a^2} + \frac{S_b^{ij}}{\rho_b^2} \right) \cdot \nabla_a W_{ab}, \tag{2}$$

where $\mathbf{v}_a = \mathbf{v}(\mathbf{r}_a)$ is the velocity of particle a, ∇_a is the gradient operator with respect to the position $\mathbf{r}_a$ of that particle, and S^{ij} are the components of the stress tensor given by

$$S^{ij} = -p\delta^{ij} + \sigma^{ij}, \tag{3}$$

where p is the internal pressure, δ^{ij} is the unit tensor, and σ^{ij} are the components of the viscous stress tensor defined as

$$\sigma^{ij} = \eta \left(\frac{\partial v^i}{\partial x^j} + \frac{\partial v^j}{\partial x^i} \right) + \left(\zeta - \frac{2}{d}\eta \right) (\nabla \cdot \mathbf{v})\, \delta^{ij}. \tag{4}$$

Here x^i denotes the ith Cartesian component of the position vector $\mathbf{r}$, v^i is the ith component of the fluid velocity, and η and ζ are the coefficients of shear and bulk viscosity, respectively. In Eq. (4), the parameter d specifies the number of spatial dimensions, that is, $d = 2$ or 3 for two- or three-space dimensions, respectively. For details on the derivation of Eq. (2) and the corresponding symmetrized SPH representation for the time rate of change of the specific internal energy, including the effects of heat conduction, we refer to [9]. In practice, it is a simple matter to calculate the viscous forces on the right-hand side of Eq. (2) since they only require direct evaluation of the viscous stress tensor (4), which in turn can be expanded in complete SPH form using the standard expressions

$$(\nabla \mathbf{v})_a = \frac{1}{\rho_a} \sum_{b=1}^{N} m_b \left(\mathbf{v}_b - \mathbf{v}_a\right) \nabla_a W_{ab}, \tag{5}$$

and

$$(\nabla \cdot \mathbf{v})_a = \frac{1}{\rho_a} \sum_{b=1}^{N} m_b \left(\mathbf{v}_b - \mathbf{v}_a\right) \cdot \nabla_a W_{ab}, \tag{6}$$

for the velocity gradients and divergence, respectively. Note that Eq. (2) can be used regardless of whether the shear and bulk viscosity coefficients are constant, as in the Navier-Stokes equations, or arbitrary varying functions of the coordinates. Since direct evaluation of second-order derivatives of the kernel is not required, the method permits the use of low-order interpolating kernels of compact support, such as the spherically symmetric cubic spline kernel proposed by Monaghan & Lattanzio [28], without compromising the stability and accuracy of the calculation, even in the case of very small Reynolds numbers [9].

Since SPH can be computationally more expensive than other alternative techniques for a given application, especially when a large number of particles is involved, a basic requirement here is that the search for nearest neighbors must be performed efficiently in order to reduce the computational cost. For applications with a constant smoothing length h, an increase in efficiency is achieved through the use of grids and linked lists [29, 30]. However, these methods are not generalizable to the case of spatially varying smoothing lengths. In particular, a variable h is desirable in applications where regions of relatively low and high density of particles coexist in the flow domain. In this case, full advantage of the particle distribution to resolve local structures can be taken by treating both types of regions with comparable accuracy. This task can be performed efficiently using the TREESPH method of Hernquist & Katz [8], which combines SPH with the hierarchical tree algorithm of Barnes & Hut [31]. Originally invented for astrophysical applications to self-gravitating systems, TREESPH solves the Poisson equation efficiently and adaptively without appealing to grid-based methods and, compared to other SPH-based schemes, optimizes the search for nearest neighbors even in applications where calculation of the gravitational forces is not required. This is possible because the Barnes-Hut tree method relies on a hierarchical subdivision of space into cubic cells, allowing for range searching and recording only the appropriate neighbors to each particle. As a result, TREESPH is able to handle individual particle smoothing lengths and individual particle timesteps, making the scheme fully adaptive in space and time. Although the method was devised for astrophysical applications, it is also applicable to a much broader class of problems involving both long- and short-range forces. Even in the case of incompressible flows, where h need not vary in space and time, TREESPH can work more efficiently than other SPH-based codes, simply because the tree method reduces to a pure nearest searching algorithm.

2.2. Treatment of solid boundaries

In problems involving flow through pipes and chokes where solid walls are present, the accuracy of the calculations is sensitive to the treatment of the interaction between the fluid and the solid surface. For simulations of a viscous fluid flow in presence of solid walls, it is necessary to impose no-slip boundary conditions to mimic the sticking of the fluid to the wall. It is common practice in SPH to model such boundary conditions using image particle methods, which in turn are useful in removing the severe crippling density deficiency that arises when Eq. (1) is applied to particles near a boundary.

In particular, we adopt here the method employed by Takeda *et al.* [17], in which image particles are created by reflecting fluid particles across the boundary. This operation results in a collection of imaginary particles which are external to the fluid domain. Such particles are treated as actual SPH particles, and so they contribute to the density and pressure gradients. In practice, accurate results for the kernel smoothing of the density are obtained by reflecting no more than four fluid particles aligned in the direction normal to the surface. Unlike actual fluid particles, imaginary particles are not allowed to move relative to the solid surface. Although a velocity is necessarily assigned to each of them, they are always constrained to remain anchored to the solid wall in the course of the calculation. In that way, each imaginary particle is given a density equal to the value of its closest image within the fluid domain. For instance, if we denote by d_i the normal distance of the imaginary particle i to the solid boundary surface, its closest image is chosen such that $|d_a - d_i|$ is a minimum, where the minimum is taken over all normal distances d_a of fluid particles a to the boundary surface. Moreover, the velocity v_i of the imaginary particle i is calculated from the value of its closest image, say v_a, using the interpolation formula

$$v_i = -v_a \frac{d_i}{d_a}. \tag{7}$$

In this way, a linear variation in the direction normal to the boundary surface is allowed to the velocity of each imaginary

particle such that it exactly vanishes of the surface. An extension of this method to curved surfaces is described in Ref. 13. Although this procedure has been found to work particularly well for plane walls and curved surfaces with a simple geometry, it is computationally expensive and fails for irregular solid boundaries. An alternative method which is able to handle solid surfaces of any shape as well as other types of boundaries, including free and deformable surfaces, in a unified manner is currently being undertaken. This new scheme is based on a modified expression for the kernel smoothing of the density and specialized SPH representations of the hydrodynamic equations for particles near a boundary, and so it may treat several types of boundaries in essentially the same manner without the need for processing imaginary particles outside the computational volume. Details of this method along with applications to a variety of different test cases, will be presented in a forthcoming paper.

2.3. Time-dependent plane Poiseuille flow

As a simple test case, we consider the unsteady incompressible flow between two infinite, parallel plates at rest. As in Ref. 9, we choose the (x,y)-plane to represent the fluid and the positive x-axis as the flow direction. The center of the channel is made to coincide with $y = 0$, so that the plates are located at $y = \pm d$ and separated by a distance $2d$. For this simple case, an analytical solution to the Navier-Stokes equations can be found for the x-velocity as a function of the y-coordinate and time t, namely

$$v_x(y,t) = \frac{F}{2\nu}\left(y^2 - d^2\right) + \sum_{n=0}^{\infty} \frac{16(-1)^n d^2 F}{\nu\pi^3(2n+1)^3} \cos\left[\frac{(2n+1)\pi y}{2d}\right] \times \exp\left[-\frac{(2n+1)^2\pi^2\nu t}{4d^2}\right], \quad (8)$$

where ν is the coefficient of kinematic viscosity and $F = \Delta p/(\rho L)$ is a force per unit mass proportional to the hydrostatic pressure gradient $\Delta p/L = -2\nu\rho v_0/d^2$ measured between two points separated by a length L along the x-direction. Here v_0 is a constant asymptotic velocity given by

$$v_0 = -\frac{F}{2\nu d^2}\,. \quad (9)$$

As $t \to \infty$, the series solution on the right-hand side of Eq. (8) vanishes and so the velocity approaches the steady-state solution given by the first term, which describes a parabolic profile with the vertex of the parabola (at $y = 0$) moving in the direction of the flow with the asymptotic velocity v_0. Thus, if at the entrance of the channel the flow is uniform, it will then evolve into a sequence of parabolic profiles until a stationary solution of the form given by the first term on the right-hand side of Eq. (8) is achieved.

The transient behavior is calculated with the TREESPH code for the case of a very low Reynolds number ($Re = 0.0125$) and taking $2d = 0.1$ cm, $\rho = 1.0$ g cm^{-3}, and $v_0 = 1.25 \times 10^{-3}$ cm s^{-1}. With this choice, the coefficient of kinematic viscosity is $\nu = 0.01$ cm^2 s^{-1}. The calculation was made using 1891 fluid particles spanning the channel from $x = 0$ to $x = L$, with $L = 0.05$ cm. The particles are initially at rest and distributed on a regular Cartesian mesh, with 31 particles along the length L and 61 covering the separation distance between the plates, yielding an interparticle distance of $\approx 1.67 \times 10^{-3}$ cm in both directions. The number of neighbors within the area enclosed by a circle of radius $2h$ is chosen to be 12, so that $h \approx 1.86 \times 10^{-3}$ cm. The presence of the bounding solid walls is handled as outlined above, by placing four consecutive rows of 31 imaginary particles each along the length L just outside the plates. Periodic boundary conditions are applied at the inlet and outlet sides of the channel by first adding four extra particles to the left ($x < 0$) and to the right ($x > L$) extremes of each row of exterior imaginary particles, thus yielding a total number of 39 imaginary particles per row, and then filling the space just ahead ($x < 0$) and behind ($x > L$) the channel with four columns of 61 imaginary particles each, covering the full separation distance between the plates along the y-direction. After each timestep, the information carried by the four columns of fluid particles next to the exit of the channel is copied into the four columns of imaginary particles next to the entrance. In this way, for each particle leaving the channel there is another one entering on the inlet side which carries its information. For convenience in handling the tree construction in the TREESPH code, the total number of particles must be conserved during the whole calculation. This is easily done by noting that, for each fluid particle leaving the channel and entering in the outlet set of imaginary particles, there will be one particle belonging to this set which is removed and placed into the inlet set to compensate for the one that enters the channel.

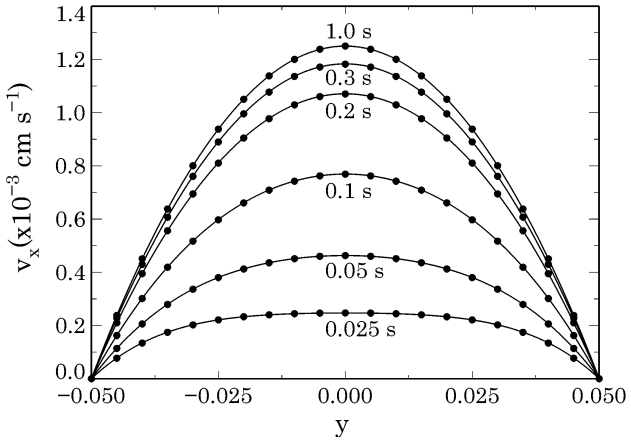

FIGURE 1. Numerically obtained velocity profiles (filled dots) compared to the analytical solution (solid curves) for unsteady Poiseuille flow between two infinite plates with $Re = 0.0125$. A sequence of times in seconds is shown for the transient evolution until 1.0 s when the steady-state solution is achieved.

The results for the transient behavior are displayed in Fig. 1, where the velocity profiles are shown for a sequence of times up to 1.0 s, when the steady-state solution has already been reached. We find that the numerical solution (filled dots) reproduces the analytical one (solid curves) given by Eq. (8) with a maximum relative error of 0.28% during the transient, while at 1.0 s it improves to 0.16%. In addition, the asymptotic value v_0 (at 1.0 s) is obtained with a relative error of $\sim 0.08\%$. The incompressibility of the fluid is also very well reproduced by the calculation, with the maximum and minimum ratios of the numerical to the analytical density being 1.0002 and 0.9999, respectively. We further note that the points of contact of the fluid with the solid walls remain fixed in space and time, a feature of the solution which is also accurately reproduced by the calculation.

3. Wellhead choke models

The aim of this paper is to present exploratory two-dimensional simulations of single-phase flow through wellhead chokes of dimensions similar to those employed in real production piping. The geometry of the wellhead choke device model is shown in Fig. 2. The system is composed of a horizontal pipe of half-length $L/2 \approx 59.27$ cm with a constriction, or choke throat, in the middle. The pipe has a radius of $D_1/2 \approx 4.45$ cm just before the choke (upstream part) and of $D_2/2 \approx 2.67$ cm after it (downstream part). A choke throat of half-length $\lambda/2 \approx 6.82$ cm and radius $\delta/2 \approx 0.593$ cm is designed in correspondence with typical real systems. Mean quantities before and after the choke throat are evaluated at the position of the dots in Fig. 2 denoted "1" and "2", respectively. As for the previous plane Poiseuille test, we choose the (x,y)-plane to represent the flow and the positive x-axis as the direction of the main flow. The pipe region is filled with a total number of 8785 fluid particles initially at rest and arranged in a uniformly spaced Cartesian mesh.

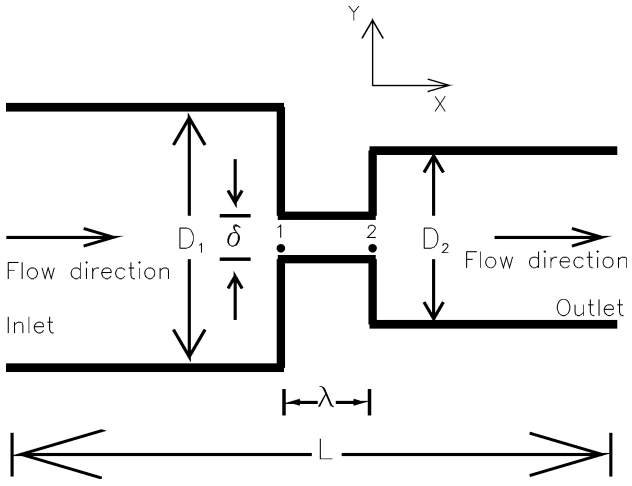

FIGURE 2. Geometry of the wellhead choke model used in the calculations. The flow within the choke system is along the x-axis in the direction of increasing x.

With this choice, the interparticle distance is about 0.296 cm along the x- and y-axes. Each fluid particle spans a circle of influence of radius $2h$ around it, giving an initial $h \approx 0.317$ cm. We assume that there is no significant heat exchange between different parts of the fluid, and that the pressure is related to the density through the isothermal equation of state

$$p = c^2 \rho, \tag{10}$$

where c is the speed of sound. For present calculations we take $c = 2.0 \times 10^4$ cm s^{-1}.

Inlet boundary conditions are designed by injecting particles at the entrance of the pipe with a Poiseuille velocity profile given by

$$v_x = v_{\rm inlet}(t)\left(1 - \frac{y^2}{R^2}\right), \qquad v_y = 0, \tag{11}$$

where t is time, R denotes the radius of the pipe, and $v_{\rm inlet}(t) = v_0(t/\tau)$ for $t \leq \tau$ and $v_{\rm inlet}(t) = v_0$ for $t > \tau$, with $\tau = 0.1$ s and $v_0 = 500$ cm s^{-1}. Thus, at $t = 0$, all particles are at rest while during the first 0.1 s, the velocity of the inlet particles is allowed to increase linearly with time until a stationary Poiseuille flow is achieved for $t \geq \tau$. In addition, the injection of particles is made at the pipe entrance such that the input density is always 1.0 g cm^{-3}.

Treatment of the solid boundaries is achieved by covering the surface of the wellhead choke device with four consecutive rows of 401 linearly arranged imaginary particles each and using the same method outlined in Sec. 2.2. With this choice, the crippling deficiency implied by the use of Eq. (1) near a solid surface is completely removed. Inlet and outlet boundary conditions are designed by first adding to each row of exterior imaginary particles 6 more particles on each side, yielding a total number of 413 particles per row, and then filling the space on the inlet side with 6 columns of 31 imaginary particles each, covering the full upstream pipe diameter, and that on the outlet side with 6 more columns of 19 imaginary particles each, covering the full downstream pipe diameter. Two distinct wellhead choke models are considered which differ only in the form of the outlet flow boundary condition. In one model, a lid with a small orifice of radius 0.44 cm and centered at $y = 0$ is placed at the outlet end ($x = L/2$) of the pipe, as shown in Fig. 2. In this way, as the flow pushes the particles downstream, some of them may eventually leave the system through the orifice. A reason for placing this further restriction is to simulate the resistance that the fluid finds after having passed through the choke throat. In practice, the lid is modeled as a solid wall and the orifice by removing three particles per column around $y = 0$ from the outlet set of imaginary particles. When a particle of the inlet set is injected at the pipe entrance, the rightmost particle that has already left the system through the orifice is removed and placed into the inlet set of imaginary particles to compensate for the one that that which entered. In this way, the total number of particles is conserved during the calculation.

In contrast, the second model mimics an infinitely long pipe downstream. In this case, the streamwise gradient for each variable is prescribed to be equal to zero at the outlet. Within the SPH framework, such boundary condition is easily implemented by using the outlet set of imaginary particles as the images of those fluid particles that are closest to the pipe exit. Therefore, each imaginary particle belonging to the outlet set is given the density and velocity of its closest image such that the streamwise density and velocity gradients vanish at $x = L/2$. When a fluid particle leaves the pipe, it is removed and stored in a reservoir of particles where it will be assigned a zero velocity. With this provision, the outflowing particles are not allowed to enter the region occupied by the outlet set of imaginary particles, and the x-coordinate of the right extreme of the computational tube is kept fixed in time at $x = L/2$. Moreover, when an inlet imaginary particle is injected into the left extreme of the tube to become a fluid particle, another one is automatically removed from the reservoir and inserted into the inlet set of imaginary particles with a prescribed input density of 1.0 g cm^{-3} and a velocity as given by Eq. (11). This guarantees that the total number of particles is strictly conserved during the calculation.

Here we consider three separate model calculations all starting with the same parameters as specified above. In all cases, the particles filling the computational domain are given an initial density equal to the input value of 1.0 g cm^{-3}. The coefficient of kinematic viscosity is assumed to be constant and equal to $\nu = 5.0 \times 10^{-4}$ cm^2 s^{-1} for two model calculations, which differ only in the form of the outlet boundary condition, *i.e.*, for one model (case A) the downstream flow is inhibited by the presence of a lid with a small orifice at the outlet end of the pipe (see Fig. 2), while for the second model (case B), an infinitely long pipe of constant cross-sectional area is allowed downstream. The third model calculation (case C) is identical to case B except that a higher coefficient of kinematic viscosity ($\nu = 0.01$ cm^2 s^{-1}) is used. For all three cases, the coefficient of bulk viscosity is set to zero.

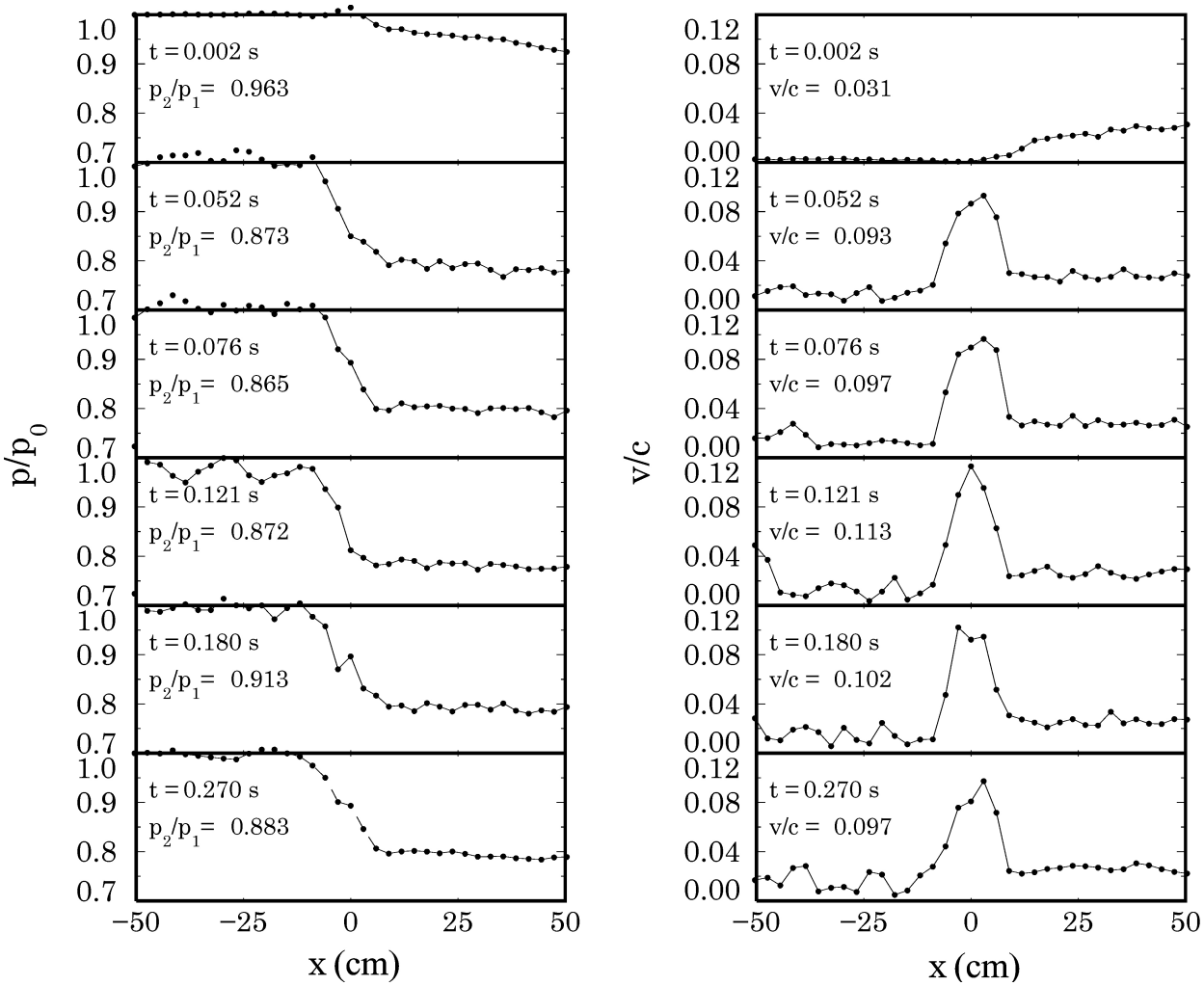

FIGURE 3. Mean pressure (left panel) and velocity (right panel) profiles across the full length of the pipe for model A. The velocity is given in units of the sound velocity c and the pressure in units of the input pressure $p_0 = c^2\rho_0$, where the input density $\rho_0 = 1.0$ g cm^{-3}. An approximate mean flow steady-state solution is achieved by the time $t = 0.052s$.

4. Results

We first describe the results for model A, which differs from the other two cases in that the downstream flow after the choke throat is inhibited by a solid lid with a small orifice placed at the outlet end $x = L/2$ of the pipe. The details of the evolution for this case are shown in Fig. 3, which depicts the mean pressure (left panel) and velocity (right panel) profiles across the full length of the tube for a sequence of times from $t = 0.002$ s to $t = 0.27$ s. The pressure is given in units of the input pressure $p_0 = c^2\rho_0$, where the input density $\rho_0 = 1.0$ g cm^{-3}.

The filled dots represent average values of the pressure and velocity. In particular, each dot on the curves is a mean value obtained by averaging over the contribution of all particles within a pipe section of area $2R\Delta x$, where $\Delta x \approx 3.39$ cm and R may be either the radius of the choke throat or that of the pipe before or after the choke. For each of the curves in Fig. 3 we present details in Table I of the mean pressure and velocity just before and after the choke and the maximum mean velocity within the choke. At the very beginning of the calculation, a flow sets in rapidly across the pipe as shown by the curve for $t = 0.002$ s, which pushes the particles downstream, making some of them leave the system through the orifice. As a result, a jet of particles is formed in the region $x > L/2$. This is shown by the mean flow velocity rising monotonically downstream and reaching a maximum value at the outlet end of the pipe. Conversely, the mean flow pressure decreases toward the outlet end. From Eq. (11) it follows that by 0.002 s the inlet velocity is only 2% of the value for true steady-state Poiseuille inflow. As the inlet velocity increases, the extension of the outer jet shrinks and eventually disappears. This occurs at about 0.052 s, when the inlet velocity is 14% of the steady-state Poiseuille value. When this happens, both the mean pressure and velocity profiles within the tube no longer change qualitatively, implying that an approximate mean flow stationary pattern is achieved. Common to all these profiles is a well-marked mean pressure drop within the choke region. In the right panel we also see that the mean flow velocity increases steeply at the entrance of the choke throat. This is one effect of the much smaller cross-sectional area available for the flow across the choke. When the flow exits the choke, its mean velocity decreases discontinuously to a value which is slightly higher than that just ahead the choke. In particular, by 0.052 s, the ratio of the mean pressure behind to that ahead of the choke throat is $p_2/p_1 \approx 0.87$, implying an approximate 13% decrease in the mean pressure in the downstream direction, while the maximum mean velocity within the choke is about $0.093c$, which is a factor of ~ 8 times higher than the value just ahead of the choke. As the evolution proceeds, the pressure ratio p_2/p_1 oscillates between ≈ 0.86 and ≈ 0.95, while the maximum mean velocity does so in the range $\approx 0.097 - 0.113c$. By 0.27 s, when the calculation is terminated, $p_2/p_1 \approx 0.88$ and the maximum mean velocity is $\approx 0.1c$. The discontinuous behavior of the mean pressure and velocity across the choke induces fluctuations in the flow which propagate downstream. while part of these waves are transmitted through the orifice, leaving the system, most of them are reflected back. The reflected waves then interact with the ones propagating downstream, causing a gradual decrease in their amplitude, as may be seen by comparing the sequence of mean pressure and velocity profiles for the downstream flow. As the reflected waves propagate back across the choke, they also affect the upstream mean flow, as evidenced by the relatively higher amplitude ripples present in the mean pressure and velocity profiles before the choke. The continual interaction between the incoming and reflected waves will then cause the amplitude of the fluctuations to gradually decrease with time.

The results for model B with an infinitely long pipe downstream are shown in Fig. 4 and Table II, where the mean pressure and velocity profiles are displayed for a sequence of times from $t = 0.0025$ s to $t = 0.298$ s. Compared to model A, an approximate mean flow stationary solution is now achieved after a longer time ($t = 0.087$ s), when the inlet velocity is 27.5% of the required value for steady-state Poiseuille flow. After this time, both the mean pressure and velocity profiles remain qualitatively similar in the course of the evolution, as shown by the sequence of Fig. 4 curves. The mean pressure drop across the choke throat corresponds to a pressure ratio $p_2/p_1 \approx 0.92$, while the maximum velocity within the choke oscillates between $\approx 0.098c$ and $0.113c$. By the time $t = 0.298$ s, the pressure drop is of about 8% compared to the 12% decrease for model A. Evidently, having a long pipe downstream with no restrictions reduces the pressure drop. In the downstream part of the pipe (after the choke) the mean flow velocity is higher by factors of ~ 1.5 compared to that in the upstream section before the choke. The ripply behavior of the profiles after the choke indicates the existence of pressure and velocity fluctuations which propagate downstream with the flow. Because of the outflowing boundary conditions, these fluctuations are never reflected back, thus explaining why the upstream mean flow profiles look much smoother compared to model A.

TABLE I. Mean pressure just before the choke (p_1) and after the choke (p_2) and mean velocity just before the choke (v_1) and after the choke (v_2) for model A for the curves shown in Fig. 3. The maximum mean velocity within the choke is $v_{\max}$, p_0 denotes the input density, c the sound speed and the time is given in seconds.

Time	p_1/p_0	p_2/p_0	p_2/p_1	v_1/c	v_2/c	$v_{\max}/c$
0.0020	1.0050	0.9681	0.9632	0.0007	0.0057	0.0307
0.0520	0.7909	0.6908	0.8734	0.0785	0.0301	0.0930
0.0760	0.7489	0.6480	0.8652	0.0841	0.0332	0.0965
0.1210	0.6895	0.6014	0.8722	0.0898	0.0237	0.1130
0.1800	0.6124	0.5590	0.9128	0.1021	0.0306	0.1021
0.2700	0.6055	0.5350	0.8835	0.0757	0.0243	0.0972

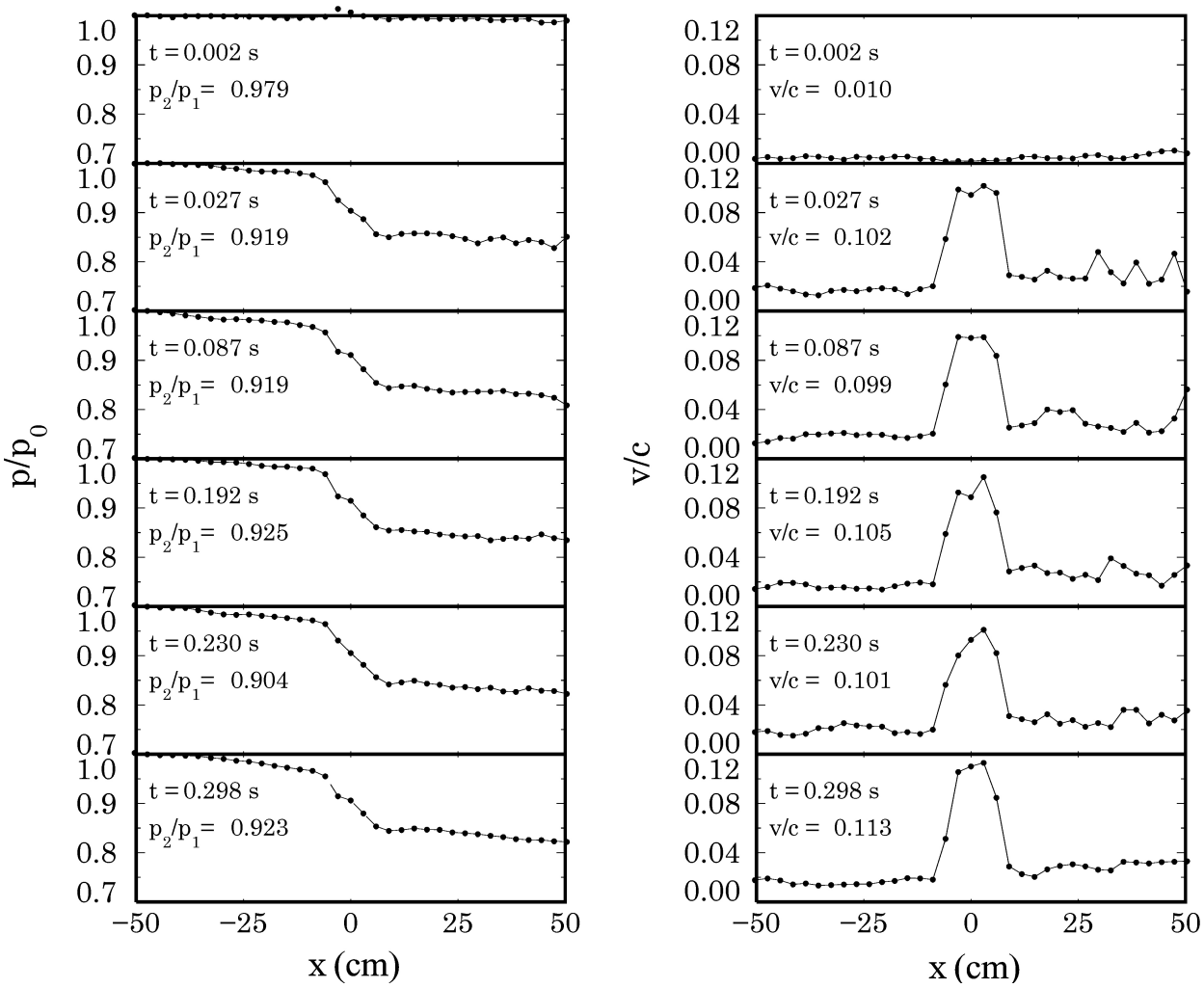

FIGURE 4. Mean pressure (left panel) and velocity (right panel) profiles across the full length of the tube for model B. The velocity is given in units of the sound velocity c and the pressure in units of the input pressure $p_0 = c^2\rho_0$, where the input density $\rho_0 = 1.0$ g cm^{-3}. An approximate mean flow steady-state solution is achieved by the time $t = 0.087$ s.

TABLE II. Mean pressure just before the choke (p_1) and after the choke (p_2) and mean velocity just before the choke (v_1) and after the choke (v_2) for model B for the curves shown in Fig. 4. The maximum mean velocity within the choke is $v_{\max}$, p_0 denotes the input density, c the sound speed and the time is given in seconds.

Time	p_1/p_0	p_2/p_0	p_2/p_1	v_1/c	v_2/c	$v_{\max}/c$
0.0025	1.0140	0.9926	0.9788	0.0018	0.0001	0.0104
0.0275	0.9868	0.9065	0.9186	0.0987	0.0291	0.1018
0.0875	0.9869	0.9074	0.9194	0.0990	0.0253	0.0990
0.1925	0.9866	0.9126	0.9249	0.0926	0.0285	0.1051
0.2300	1.0000	0.9042	0.9042	0.0802	0.0309	0.1011
0.2975	0.9816	0.9061	0.9230	0.1055	0.0288	0.1130

Finally, in Fig. 5 and Table III we display the results obtained for model C, which is identical to case B except that the coefficient of kinematic viscosity is increased by a factor of 20. In this case, an approximate mean flow stationary solution is reached by $t = 0.085$ s, when the inlet velocity is 32.5% of the steady-state Poiseuille flow value. Also, the value of the mean flow velocity at the exit of the choke is a factor of ~ 1.7 higher compared to the corresponding value at the choke entrance. Except for these quantitative differences, the mean pressure and velocity profiles are very similar to those shown in Fig. 4, with $p_2/p_1 \approx 0.92$ and maximum mean velocities of about $0.1c$ across the choke. Thus, enhancing the viscous properties of the fluid has little effects on the pressure drop and velocities within the choke region.

As an example of the flow structure, we present in Fig. 6 the velocity field of model C at $t = 0.295$ s. The top and bottom panels give the velocity field for the upstream and downstream sections of the channel, respectively, while the middle panel is an enlargement of the flow structure through the choke throat. In the upstream section, the flow is accelerated in front of the choke because of the restricted cross-sectional area. The flow velocity decays in the proximity of solid walls where the fluid sticks due to viscous effects. In the downstream section, a jet forms which then extends along the full length of the channel, as shown in Fig. 6c.

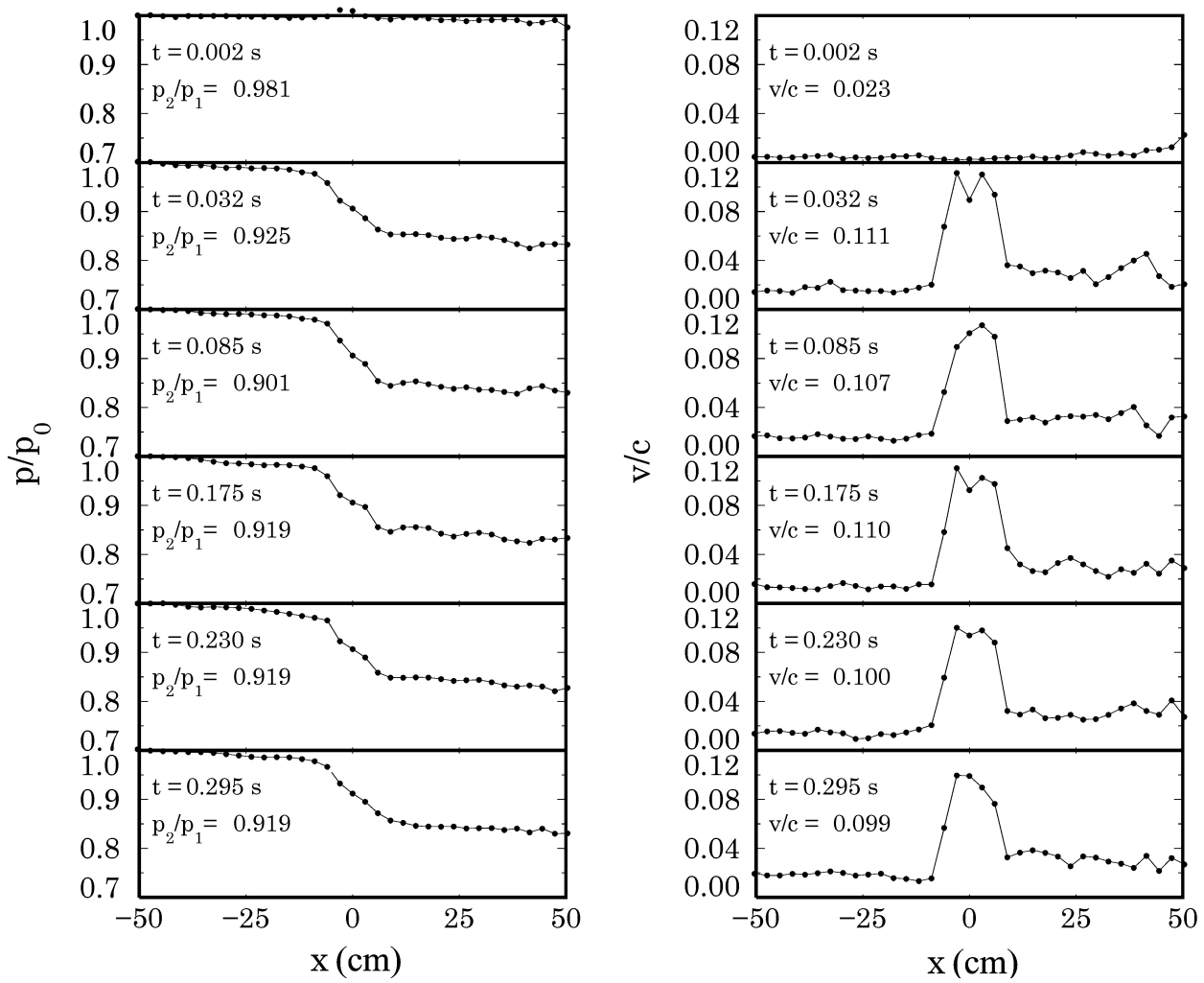

FIGURE 5. Mean pressure (left panel) and velocity (right panel) profiles across the full length of the tube for model C. The velocity is given in units of the sound velocity c and the pressure in units of the input pressure $p_0 = c^2\rho_0$, where the input density $\rho_0 = 1.0$ g cm^{-3}. An approximate mean flow steady-state solution is achieved by the time $t = 0.085$ s.

TABLE III. Mean pressure just before the choke (p_1) and after the choke (p_2) and mean velocity just before the choke (v_1) and after the choke (v_2) for model C for the curves shown in Fig. 5. The maximum mean velocity within the choke is $v_{\max}$, p_0 denotes the input density, c the speed of sound and the time is given in seconds.

Time	p_1/p_0	p_2/p_0	p_2/p_1	v_1/c	v_2/c	$v_{\max}/c$
0.0025	1.0114	0.9920	0.9807	0.0018	0.0039	0.0225
0.0325	0.9858	0.9122	0.9253	0.1114	0.0361	0.1114
0.0850	1.0021	0.9032	0.9012	0.0894	0.0288	0.1071
0.1750	0.9868	0.9068	0.9189	0.1103	0.0451	0.1103
0.2300	0.9887	0.9092	0.9195	0.1001	0.0321	0.1001
0.2950	0.9971	0.9164	0.9190	0.0994	0.0325	0.0994

Our results may apply to subcritical flow of an isothermal gas through wellhead chokes; however, a direct comparison with the experimental curves reported by Fortunati [2], who derived the dependence of the velocity through the choke on the pressure ratio p_2/p_1 for gas-oil mixtures with different gas concentrations, including pure gas, is not possible because of the simplified equation of state used in this investigation. For models B and C, the present calculations predict on average pressure ratios of ≈ 0.92 and velocities in the range $0.098 - 0.113c$ across the choke. For pure natural gas with a sound speed of 29300 cm s^{-1}, the above velocities correspond to about (2871 - 3311) cm s^{-1}. For this range of velocities, the experimental curve derived by Fortunati [2] (see his Fig. 2, curve 1) yields $p_2/p_1 \approx 0.97$ - 0.98, which is higher than the average ratio of ≈ 0.92 predicted by the present models. A better fit with the experimental results would then require using more realistic equations of state. Of particular interest is the simulation of gas-oil mixtures through wellhead chokes. According to the experimental data available [2, 6], for flow velocities of the order of (2000 - 4000) cm s^{-1} through wellhead chokes, the pressure drop is seen to significantly increase for gas-oil mixtures compared to the case of pure gas.

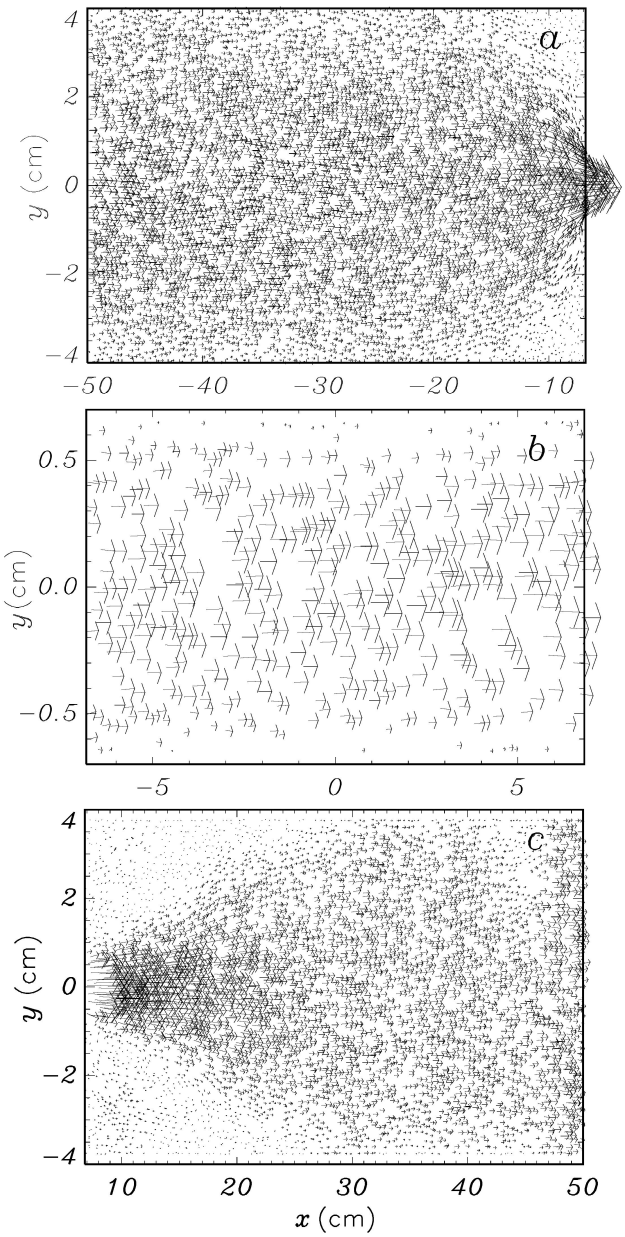

FIGURE 6. Velocity flow field for model C at $t = 0.295$ s. The top (a) and bottom (c) panels gives the velocity field for the upstream and downstream sections of the channel, respectively, while the middle panel (b) is an enlargement of the flow structure through the choke throat. The maximum velocity is $\approx 0.1c$.

5. Conclusions

We have performed exploratory two-dimensional model calculations of single-phase flow through a wellhead choke of a dimensions similar to those installed in real production piping using the Smoothed Particle Hydrodynamics (SPH) method. As a first approximation, we have assumed that negligible heat transfer occurs between different parts of the fluid and so the models were carried out using an isothermal equation of state. The choice of the geometry and parameters are such that the models are well suited to describing the flow of gas through a pipe with a choke throat in the middle.

Three different models were considered which differed either in the form of the outlet boundary condition or the value of the constant coefficient of kinematic viscosity. In the first model, the pipe is designed by placing a lid with a small orifice at its end in order to inhibit the outlet flow, while the other two models, differing only in the value of the kinematic viscosity, allow for an infinitely long pipe downstream. In all cases, the inlet conditions correspond to Poiseuille flow with a constant density. The results for these model calculations indicate that the mean flow achieves an approximate steady state in a very short timescale. The stationary solution is always characterized by a well-pronounced drop in the mean density and pressure through the choke throat. At the entrance to the choke, the mean flow velocity increases steeply, reaching typical values which are on average factors of ~ 5 to ~ 6 times higher than those for the upstream flow. The mean flow velocity also decreases steeply at the choke exit, dropping to downstream values that are slightly higher compared to those for flow in the upstream section of the pipe. The flow across the choke throat always remains subsonic with typical velocities of about $0.1c$. In particular, when the flow is inhibited downstream, the mean pressure drop is of about 12% and decreases to $\sim 8\%$ or less when the entire outlet cross-section of the tube is free of any restrictions. Experimental available measurements and correlations for natural gas flowing across wellhead chokes indicate that for speeds of $\sim 0.1c$, the ratio of the pressure before to that after the choke may be as high as 0.97 - 0.98, implying a lower pressure drop than predicted by the present calculations. A direct comparison of the results with the available experimental data will certainly be possible for more realistic equations of state.

The present two-dimensional calculations represent a step ahead in consistently simulating choked flow systems. The development of a three dimensional parallel multiphase SPH code with sophisticated physics and for irregular geometries is under way. In the new scheme we replace the use of image particles by a method that uses a color index for correcting interpolating errors near boundaries, detecting the presence of boundaries, obstacles or the interphase between two fluids and for calculating tension forces. Further details will be given elsewhere.

Acknowledgments

We thank an anonymous referee for suggestions that improved the final version of the manuscript. One of us (J.K.) is grateful to Federico Gonzalez Tamez of PEMEX, who introduced me to the interesting problem of flow through wellhead chokes. The calculations in this paper were performed using the Silicon Graphics Altix 350 computer system of the Instituto Nacional de Investigaciones Nucleares (ININ) of Mexico. This work is partially supported by the Mexican Consejo Nacional de Ciencia y Tecnología (CONACyT) under contracts U43534-R and J200.476/2004, the Fondo Nacional de Ciencia, Tecnología e Innovación (Fonacit) of Venezuela, the German Deutsche Forshungsgemainshaft (DFG) and the German Deutscher Akademischer Austauschdienst (DAAD).

1. N.C.J. Ros, *Appl. Sci. Rev.* **9** (1960) 374.
2. F. Fortunati, "Two-phase flow through wellhead chokes", in The SPE-European Spring Meeting 1972 of the Society of Petroleum Engineers of AIME, SPE 3742, (Amsterdam, The Netherlands, May 1972) p. 16.
3. F.E. Ashford, *J. Pet. Tech.* (1974) August 843.
4. F.E. Ashford and P.E. Pierce, *J. Pet. Tech.* September (1975) 1145.
5. G.H. Abdul-Majeed, "Correlations developed to predict two phase flow through wellhead chokes", in The 1988 Petroleum Society of CIM, Annual Technical Meeting, CIM 88-39-26, Calgary, (Canada, June 1988) p. 12.
6. T.K. Perkins, *SPE Drilling & Completion* December (1993) 271.
7. J. Klapp, G. Mendoza, L. Di G. Sigalotti, and E. Sira, "Numerical simulations of flow through wellhead chokes with the Smoothed Particle Hydrodynamics method", in 7th World Conference on Systematics, Cybernetics and Informatics, SCI 2003, (Orlando, USA, July 2003) p. 27.
8. L. Hernquist and N. Katz, *Astrophys. J.* **70** (1989) 419.
9. L. Di G. Sigalotti, J. Klapp, E. Sira, Y. Meleán, and A. Hasmy, *J. Comp. Phys.* **191** (2003) 622.
10. L.D. Libersky, A.G. Petschek, T.C. Carney, J.R. Hipp, and F.A. Allahdadi, *J. Comp. Phys.* **109** (1993) 67.
11. O. Flebbe, S. Münzel, H. Herold, H. Riffert, and H. Ruder, *Astrophys. J.* **431** (1994) 754.
12. S.J. Watkins, A.S. Bhattal, N. Francis, J.A. Turner, and A.P. Whitworth, *Astron. Astrophys. Suppl. Ser.* **119** (1996) 177.
13. J.P. Morris, P.J. Fox, and Y. Zhu, *J. Comp. Phys.* **136** (1997) 214.
14. J. Bonet and T.-S.L. Lok, *Comp. Meth. Appl. Mech. Eng.* **180** (1999) 97.
15. L.D. Sigalotti, H. López, A. Donoso, E. Sira, and J. Klapp, *J. Comp. Phys.* **212** (2006) 124.
16. L.D. Sigalotti and J. Klapp, *International Journal of Modern Physics D* **10** (2001) 115.
17. H. Takeda, S.M. Miyama, and M. Sekiya, *Prog. Theoret. Phys.* **92** (1994) 939.
18. L.B. Lucy, *Astron. J.* **83** (1977) 1013.
19. R.A. Gingold and J.J. Monaghan, *Mon. Not. R. Astron. Soc.* **181** (1977) 375.
20. J.J. Monaghan and J.C. Lattanzio, *Astron. Astrophys.* **158** (1986) 207.
21. J.C. Lattanzio and R.N. Henriksen, *Mon. Not. R. Astron. Soc.* **232** (1988) 565.
22. M.B. Davies, M. Ruffert, W. Benz, and E. Müller, *Astron. Astrophys.* **272** (1993) 430.
23. R.S. Klessen, A. Burkert, and M.R. Bate, *Astrophys. J.* **501** (1998) L205.
24. S. Kitsionas and A.P. Whitworth, *Mon. Not. R. Astron. Soc.* **330** (2002) 129.
25. J.J. Monaghan, *J. Comp. Phys.* **110** (1994) 399.
26. O. Kum, W.G. Hoover, and H.A. Posch, *Phys. Rev. E* **52** (1995) 4899.
27. S. Nugent and H.A. Posch, *Phys. Rev. E.* **62** (2000) 4968.
28. J.J. Monaghan and J.C. Lattanzio, *Astron. Astrophys.* **149** (1985) 135.
29. R. W. Hockney and J. W. Eastwood, *Computer simulation using particles*, 1st ed. (McGraw-Hill, New York, 1981).
30. J.J. Monaghan, *Proc. Astron. Soc. Australia* **5** (1983) 182.
31. J. Barnes and P. Hut, *Nature* **324** (1986) 446.